GRAPHENE OXIDE/POLYVINYL ALCOHOL COMPOSITE HYDROGELS WITH RADIAL STRUCTURE FOR SOLAR STEAM GENERATION

Xiaomeng Zhao[1,*], Kit-Ying Chan[1], Xiuli Dong[1], Ling Liu[1] and Xi Shen[1,2]

[1] Department of Aeronautical and Aviation Engineering, The Hong Kong Polytechnic University, Hung Hom, Kowloon, Hong Kong SAR, China
[2] Research Institute for Sports Science and Technology, The Hong Kong Polytechnic University, Hung Hom, Kowloon, Hong Kong SAR, China
*Email: xiaomeng.zhao@connect.polyu.hk

Keywords: *Composite hydrogel, solar steam generation, graphene*

ABSTRACT

Solar-powered interfacial evaporation is an important approach for solving the issue of freshwater scarcity. However, its practical application is often limited by slow water transport, inadequate thermal insulation, poor salt resistance, and the need for a foam to keep the evaporator afloat. Herein, inspired by the structures of tree roots, we develop a self-floating, boat-shaped aerogel with radial structures which not only achieves both fast water supply and thermal insulation, but also delivers excellent salt resistance. The design utilizes a synergistic effect between photothermal carbon fillers and surface structures to absorb a broad spectrum of sunlight, resulting in an aerogel with a solar absorption rate of 93%. The hydrophilic, radial, gradient channels facilitate fast absorption and transport of water to the evaporation surface. Meanwhile, the extremely low thermal conductivity of the aerogel reduces heat loss to the underlying bulk water. Therefore, the aerogel delivers an evaporation rate of 2.24 $kgm^{-2}h^{-1}$ under one sun with an energy efficiency of 85%. In addition, the boat shape enables prolong self-floating on simulated seawater with excellent salt resistance. This work provides an effective design towards practical application of highly efficient solar evaporators.

1 INTRODUCTION

The global water shortage is becoming a prominent problem especially in developing regions.[1] Seawater has an immense potential for addressing the global water shortage problem given the massive area of ocean on the earth.[2,3] Nonetheless, seawater cannot be directly used by human for drinking and most industrial applications due to its high salinity, necessitating the development of desalination technology. At the same time, solar energy is an abundant and renewable energy source, which can be converted to heat and directly utilized for solar-powered evaporation for simple desalination.[4-7] Compared to existing technologies, solar-powered evaporation does not consume additional energy other than solar energy and does not require large infrastructure to implement.

Early solar-powered evaporation techniques involve using optically concentrated sunlight to heat up a large volume of water, resulting in low efficiency due to significant heat loss to the bulk water and surrounding environment.[8-10] To address this issue, recent efforts have been made to confine heat only to the thin surface layer of the water being evaporated, which greatly reduced the thermal loss and improved the overall conversion efficiency.[11] Solar-powered interfacial evaporation uses afloat solar evaporators to fully absorb and convert solar energy into heat, which is then used to vaporize water in the interfacial region between water and air.[12-14] This localized heating approach is more efficient than conventional solar evaporation technology which directly heats the bulk water.[15] To achieve a high evaporation rate and maximize solar-to-vapor conversion efficiency, the evaporator needs to meet three requirements: (i) a high optical absorption across the full solar spectrum; (ii) an optimized heat management to minimize heat loss; and (iii) fast water transport channels to ensure sufficient water supply to the evaporation surface.

Based on the above requirements, three-dimensional (3D) evaporators having highly porous structures have been constructed from various photothermal building blocks.[16-18] Carbon-based materials such as carbon black,[19] carbon nanotubes (CNTs),[20] graphene oxide (GO),[18] reduced graphene oxide (rGO),[21] and biochar [22] are ideal photothermal materials due to their cost-

effectiveness, abundance, stability, and broadband absorption. For example, CNTs absorbed strongly in the visible and near infrared (NIR) regions.[23] Nevertheless, the hydrophobic nature of CNTs make them rather difficult to be dispersed in aqueous solutions. By contrast, GO contains abundant hydrophilic oxygenated functional groups on its surface. A combination of CNTs and GO could enhance the stability of CNT dispersions and in turn improve the efficiency of light absorption of the resulting evaporators.[24,25]

In addition to achieving high sunlight absorption through the selection of photothermal materials, rational design of the 3D structure is crucial to efficient water supply and thermal management.[26-28] To accelerate water transport, 3D structures were often designed with vertically aligned channels to directly pump water to the evaporation surface.[29-31] However, the vertical channel walls inevitably exacerbated heat loss to the bulk water, lowering the overall efficiency of the evaporator. In order to effectively reduce heat loss, double-layered structures consisting of an upper photothermal layer for efficient sunlight absorption and a lower porous layer for thermal insulation have been proposed.[32-35] Although the bottom insulation layer suppressed the heat loss by virtue of its low thermal conductivity while also served a dual purpose of water transport,[36] double-layer evaporators are often not suitable for large-scale applications due to complex, time-consuming, and expensive manufacturing.

Here, inspired by the rapid water pumping of tree roots, we designed a boat-shaped aerogel with radial porous channels through a freeze-casting technique. The incorporation of GO nanosheets and CNTs not only synergistically achieved a high absorption towards the whole solar wavelengths but also facilitated their dispersion in a polyvinyl alcohol (PVA) matrix. The GO-CNT/PVA mixture was assembled by a radial freeze-casting technique to obtain a 3D structure consisting of radial lamellar channels with porous walls. The radial channels, mimicking the structure of tree roots, quickly pumped water from the surrounding to the evaporation surface while the porous walls enabled vapor escape. The boat-shaped radial aerogel achieved an evaporation rate of up to 2.24 kg m^{-2} h^{-1} under one sun, with an energy efficiency of 85%. The evaporation rate remained stable for an extended period thanks to the excellent salt resistance of the aerogel evaporator in high-concentration saline solutions, indicating great potential for practical desalination applications.

2 EXPERIMENTAL

2.1 Fabrication of GO-CNT/PVA Composite Aerogels

The boat-shaped aerogels with radial structures were fabricated by radial freeze-casting followed by freeze-drying. First, 10.0 g PVA powders were dissolved in 100 g DI water at 130 °C for 2 h. Then, the GO solution and CNT powders were mixed at a ratio of 7:3 and stirred continuously for 3 h followed by ultrasonication for 0.5 h at room temperature until a uniform GO-CNT dispersion was obtained. Subsequently, the required amount of PVA solution was added to the above GO-CNT dispersion, and the mixture was continuously stirred at room temperature for 3 h to obtain a GO-CNT/PVA mixture solution.

To construct the boat-shaped radial structure, a hollow cylindrical copper mold was made with its bottom and half of its volume filled by polydimethylsiloxane (PDMS)**.**The mold was immersed in liquid nitrogen to generate a temperature gradient from peripherals to the center, giving rise to radial growth of ice crystals (Figure 1).The frozen samples were freeze-dried at − 50 °C for 48 h to obtain the boat-shaped GO-CNT/PVA aerogels with radial structures. Finally, the aerogels were washed with deionized (DI) water for several times and fully swollen in DI water for 3 days before evaporation tests. Two other aerogels with the same composition but different morphologies, namely, random and vertically aligned porous structures, were also prepared according to well-established freeze-casting methods for comparison.

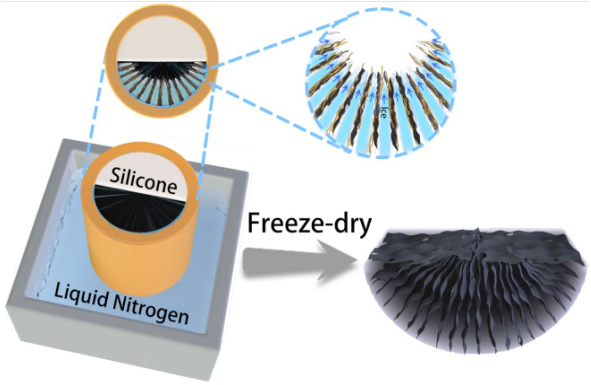

Figure 1. Fabrication of boat-shaped aerogel with radially aligned pore channels.

2.2 Solar-Powered Water Evaporation Tests

To systematically compare the evaporation performance of aerogels with different structures, a series of water evaporation tests were conducted at a relative humidity of 50% and ambient temperature. The aerogel sample was floated on the water surface in a glass beaker with the surrounding water being covered with a polyethylene (PE) foam to avoid the direct evaporation of bulk water. The sample was continuously illuminated by a solar simulator (CEL-S500/350) for 1 h under various solar intensities measured by a solar power meter (TES-1333R). The mass loss of water was recorded in real-time by an electronic balance (FA2004, 0.1 mg). The solar-to-vapor conversion efficiency was calculated by Equation (1)[5]:

$$\eta = \frac{\dot{m}\,\Delta H_{equ}}{C_{opt}\,P_o} \tag{1}$$

where $\dot{m}$ represents the water evaporation rate at a steady state, ΔH_{equ} is the equivalent vaporization enthalpy of the water from the aerogel evaporator, C_{opt} is the optical concentration, and P_O represents the normal solar density of one sun (1 kW m^{-2}).

3 RESULTS AND DISCUSSION

3.1 Biomimetic Design and Structures of GO-CNT/PVA Aerogels

Trees, as abundant biological resources on the earth, rely on their outgrown root systems to pump water and minerals from all directions under the soil and then transport continuously up through the vertical trunk to the leaves for photosynthesis. While myriad efforts have been made to develop evaporators with vertical channels inspired by tree trunks, little attention has been paid to the root system with the most water absorbing capacity.[30,37-39] Inspired by structures of tree roots, we fabricated GO-CNT/PVA aerogels with radial channels for efficient water transport (Figure 2) by using a radial freeze-casting technique. Meanwhile, the aerogel had a round bottom similar to the hull of a boat, contributing to stable floating on water without support such as foams.

Figure 2. Schematic diagram of tree-root-inspired boat-shaped aerogel using for solar-powered interfacial evaporator.

3.2 Thermal Managements of GO-CNT/PVA aerogels

As a prerequisite of the whole interfacial solar-vapor process, the aerogel needs to absorb the incident solar flux and convert to thermal energy effectively. Therefore, broadband light adsorption and a low thermal conductivity are required to maximize the solar-thermal efficiency. The light absorption capabilities of GO-CNT/PVA aerogels having three different structures, namely radially, vertically, and randomly aligned pore channels, were evaluated by measuring the absorption spectra in the solar wavelengths from 0.3 to 2.5 μm, as shown in Figure 3a. All aerogel samples were in a wet state for absorption measurements to reflect their hydrous states during the actual evaporation process. The three aerogel structures all showed high solar-weighted absorption thanks to the excellent photothermal properties of GO and CNTs, reaching 93%, 91%, and 87% for the radial, vertical, and random structures, respectively. The excellent solar absorption led to rapid rises of surface temperatures from 23 °C to around 36 °C in 10 min under one-sun solar irradiation for all aerogels, as shown in Figure 3b. With the increase of irradiation time, the steady-state temperature of the radial aerogel reached 40.6 °C, 5.7% and 9.1% higher than those of the vertical and random aerogels, respectively. The temperatures of bulk water below the aerogels were also recorded to evaluate the thermal insulation performance, as shown in Figure 3c. After one hour of exposure under one sun, the temperatures of bulk water beneath the random and vertical aerogels were elevated by 2 and 2.5 °C, respectively, because of the heat loss from the evaporation surface to the bulk water. By contrast, the temperature rise was only 1.1 °C for bulk water below the radial aerogel, indicating less severe heat loss thanks to the radial structure. The less heat loss of radial aerogel was attributed to the better thermal insulation performance arising from the radially arranged pore walls, limiting the heat transport in the transverse to pore alignment direction. In addition, the mass changes of water for different aerogel evaporators after 1 h of exposure under one-sun illumination were measured, as shown in Figure 3d. When the boat-shaped radial aerogel was used as the evaporator, the evaporation rate was 2.24 kg m^{-2} h^{-1}, which was 5.6 times that of pure water. Under the same lighting conditions, the evaporation rates of aerogels with vertical and random structures were only 69.1% and 52.7% that of the boat-shaped radial counterpart. The calculated solar-to-vapor conversion efficiencies of aerogels with different structures are shown in Figure 3e. The boat-shaped radial aerogel had an evaporation rate of 2.24 kg m^{-2} h^{-1} and an energy efficiency of 85% under one sun, both of which were higher than random and vertical aerogels.

The evaporation rates of boat-shaped radial aerogel under different solar intensities were also measured, as shown in Figure 3f. The evaporation rate rose with the increasing light concentration and reached as high as 6.25 kg m^{-2} h^{-1} under 5-sun irradiation. It is worth noting that even under weaker irradiation (0.5 sun), the evaporation rate still maintained at 1.01 kg m^{-2} h^{-1}, making the aerogel suitable for practical desalination under weak sunlight. There are several possible mechanisms responsible for the excellent evaporation performance of the boat-shaped radial aerogel: 1) The high sunlight absorption of the aerogel increases the initial energy input in the whole evaporation process; 2) The low longitudinal thermal conductivity of the aerogel effectively blocked the heat conduction to the bulk water and reduce heat loss; 3) The PVA networks weakened the interaction between water molecules and significantly reduced the evaporation enthalpy of water; and 4) The radially aligned pore walls accelerated the transport of water to the evaporation surface.

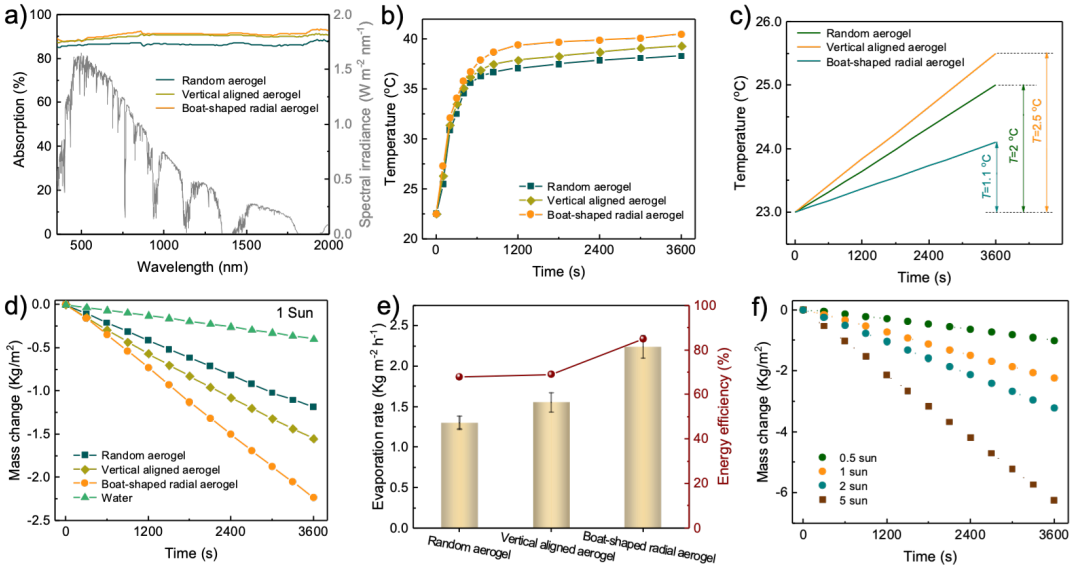

Figure 3. (a) Solar spectrum and UV–vis–NIR absorption spectra of different aerogel structures; (b) changes of surface temperature with time under 1-sun illumination; (c) temperature changes of bulk water under aerogels with different structures; (d) the mass changes of water over time under one-sun illumination, including pure water, aerogels with radial, vertical, and random structures; (e) the evaporation rates and energy efficiencies of three different aerogels; and (f) the mass changes of boat-shaped radial aerogel under different light intensities.

3.3 Salt Resistance and Long-Term Stability

In the actual desalination process, salts could accumulate in the evaporator especially for brine with high salinity, reducing the evaporation rate or even incapacitating the evaporator. Therefore, avoiding salt accumulation is the key to realize efficient and stable evaporation under high salinity. The effectiveness of boat-shaped radial aerogels in solar desalination was verified under one-sun illumination. Because the salt concentration in industrial wastewater may be higher than that in seawater, the evaporation rates in NaCl solutions with salinity ranging from 0 to 20 wt% were tested (Figure 4a). Compared with pure water, the evaporation rates in salt waters were slightly decreased. Notwithstanding, even in a 20 wt% NaCl solution, the evaporation rate still reached 1.94 kg $m^{-2}h^{-1}$, indicating a negligible effect of salts on the desalination performance. To further verify the contribution of the boat-shaped radial structure to salt resistance, the evaporation performance of the radial aerogel was compared to the random aerogel in 20 wt% high-salinity brine, as shown in Figure 4b. The evaporation rate of random aerogel began to decrease gradually after 3 h of evaporation. After 8 h of evaporation, the surface of random aerogel was completely covered by salt crystals (Figure 4c), leading to a significant drop in the evaporation rate to only 0.8 kg m^{-2} h^{-1}. In contrast, the evaporation rate of boat-shaped radial aerogel remained relatively stable with no salt accumulation on the evaporation surface throughout the 8-h evaporation measurements. The above comparison signifies the positive role of the radial structure in avoiding salt accumulation thanks to the gradient channels.

In addition, the long-term performance of boat-shaped radial aerogel was also demonstrated. The boat-shaped radiant aerogel was tested in a NaCl solution with 3.5 wt% salinity to simulate the salt concentration of seawater. The measurements were conducted for 12 hours under one sun follow by exposure in dark for another 12 hours to simulate the alternation of day and night in a cycle, which lasted for 7 days in total. As shown in Figure 4d, the evaporation rates fluctuated slightly from 1.89 to 2.22 kg m^{-2} h^{-1} during the 7-day period, averaging at 2.1 kg m^{-2} h^{-1}. This value was very close to the one obtained in the short-term evaporation test of pure water (Figure 3e), demonstrating that the boat-shaped radial aerogel can work stably in seawater-like brine for a prolonged period. Moreover, the concentrations of four major ions (Na^+, K^+, Mg^{2+} and Ca^{2+}) in the water were reduced by two to three orders of magnitude after evaporation, fully compliant with the World Health Organization (WHO) recommended drinking

water standard. These results demonstrate the reliable long-term stability and great potential for practical application of boat-shaped radial aerogels in solar-powered desalination and purification.

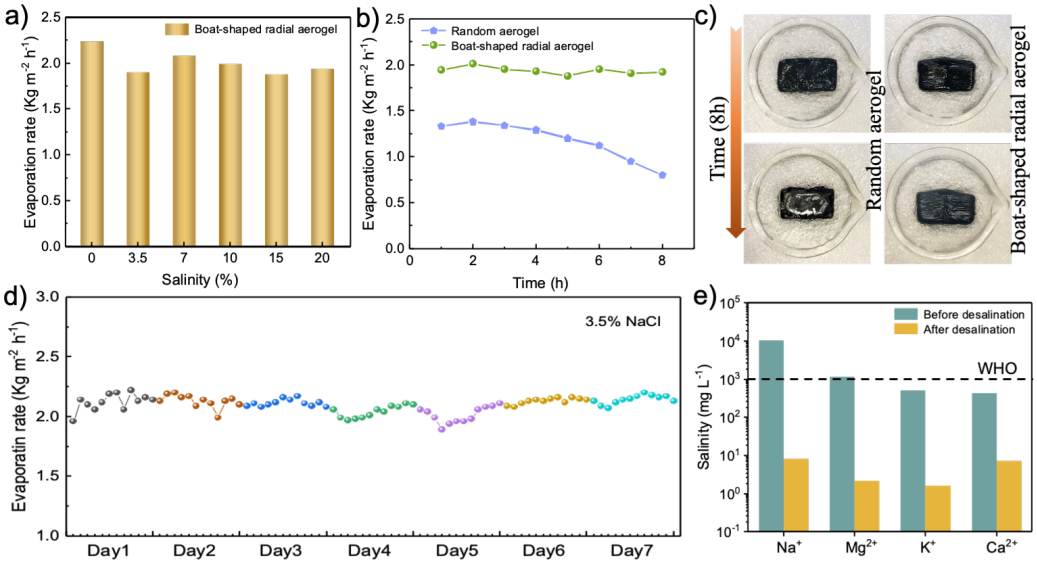

Figure 4. (a) The evaporation rates of boat-shaped radial aerogel at different salinities. (b) The changes in evaporation rates of random and boat-shaped radial aerogels in 20 wt% brine under one-sun illumination for 8 h. (c) Photographs of salt precipitation on the surfaces of random and boat-shaped radial aerogels in 20 wt% brine before and after 8-h evaporation tests. (d) Long-term evaporation rates of boat-shaped radial aerogel in a 3.5 wt% brine under one-sun illumination. (e) The concentrations of four major ions in water before and after desalination. Black dash line represents the thresholds recommended by the WHO for drinking water.

4 CONCLUSION

In summary, a self-floating aerogel evaporator with a boat-shaped radial structure was fabricated by the radial freezing-cast method for highly efficient solar-powered interfacial evaporation. First, 2D GO nanosheets and 1D CNTs synergistically contribute to a high solar absorption of 93% in the aerogel. Then, taking inspiration from tree roots, radial water transport channels with gradient channel sizes was thoughtfully designed to facilitate quick absorption of water from the surrounding and fast transport to the evaporation surface. Combined with the porous surface to allow steam outflow, the boat-shaped radial aerogel achieved an evaporation rate of 2.24 kg m^{-2} h^{-1}under one sun. Moreover, the low vertical thermal conductivity of the boat-shaped radial aerogel prevented the absorbed heat from being transferred to the underlying bulk water, thus ensuring that the heat is retained on the evaporating surface, achieving a high energy efficiency of 85%. In addition, the boat-shaped radial aerogel had excellent salt resistance and long-term stability, with no salt deposition occurring even in the 20 wt% brine after 8-h operation under one sun. Our work provided new insights into the practical application of high-performance solar evaporators, which can achieve efficient evaporation without complex structures.

ACKNOWLEDGEMENTS

This project was financially supported by the Research Grants Council (16200720and the start-up fund for new recruits of PolyU (P0038855 and P0038858).

REFERENCES

[1] M. A. Shannon, P. W. Bohn, M. Elimelech, J. G. Georgiadis, B. J. Marinas and A. M. Mayes, Science and technology for water purification in the coming decades, *Nature*, **452**, 2008, pp. 301-310 (doi:10.1038/nature06599).

[2] S. Rahmstorf, Ocean circulation and climate during the past 120,000 years, *Nature*, **419**, 2002, pp. 207-214 (doi: 10.1038/nature01090).
[3] M. Elimelech and W. A. Phillip, The future of seawater desalination: Energy, technology, and the environment, *Science*, **333**, 2011, pp. 712-717 (doi:10.1126/science.1200488).
[4] F. Zhao, X. Zhou, Y. Shi, X. Qian, M. Alexander, X. Zhao, S. Mendez, R. Yang, L. Qu and G. Yu, Highly efficient solar vapour generation *via* hierarchically nanostructured gels, *Nature Nanotechnology*, **13**, 2018, pp. 489-495 (doi:10.1038/s41565-018-0097-z).
[5] H. Zhang, X. Shen, E. Kim, M. Wang, J. H. Lee, H. Chen, G. Zhang and J. K. Kim, Integrated water and thermal managements in bioinspired hierarchical MXene aerogels for highly efficient solar-powered water evaporation, *Advanced Functional Materials*, **32**, 2022, pp. 2111794 (doi:10.1002/adfm.202111794).
[6] M. Zou, Y. Zhang, Z. Cai, C. Li, Z. Sun, C. Yu, Z. Dong, L. Wu and Y. Song, 3D printing a biomimetic bridge-arch solar evaporator for eliminating salt accumulation with desalination and agricultural applications, *Advanced Materials*, **33**, 2021, pp. e2102443 (doi:10.1002/adma.202102443).
[7] M. Zhu, Y. Li, G. Chen, F. Jiang, Z. Yang, X. Luo, Y. Wang, S. D. Lacey, J. Dai, C. Wang, C. Jia, J. Wan, Y. Yao, A. Gong, B. Yang, Z. Yu, S. Das and L. Hu, Tree-inspired design for high-efficiency water extraction, *Advanced Materials*, **29**, 2017, pp. 1704107 (doi:10.1002/adma.201704107).
[8] Z. Li, X. Xu, X. Sheng, P. Lin, J. Tang, L. Pan, Y. V. Kaneti, T. Yang and Y. Yamauchi, Solar-powered sustainable water production: State-of-the-art technologies for sunlight-energy-water nexus, *ACS Nano*, **15**, 2021, pp. 12535-12566 (doi:10.1021/acsnano.1c01590).
[9] F. Zhao, Y. Guo, X. Zhou, W. Shi and G. Yu, Materials for solar-powered water evaporation, *Nature Reviews Materials*, **5**, 2020, pp. 388-401 (doi:10.1038/s41578-020-0182-4).
[10] S. Wang, Y. Niu, W. Mu, Z. Zhu, H. Sun, J. Li, W. Liang and A. Li, Robust hollow glass microspheres-based solar evaporator with enhanced thermal insulation performance for efficient solar-driven interfacial evaporation, *Materials Today Chemistry*, **26**, 2022, pp. 101042 (doi:10.1016/j.mtchem.2022.101042).
[11] Y. Zhang, T. Xiong, D. K. Nandakumar and S. C. Tan, Structure architecting for salt-rejecting solar interfacial desalination to achieve high-performance evaporation with *in situ* energy generation, *Advanced Science*, **7**, 2020, pp. 1903478 (doi:10.1002/advs.201903478).
[12] T. Li, H. Liu, X. Zhao, G. Chen, J. Dai, G. Pastel, C. Jia, C. Chen, E. Hitz, D. Siddhartha, R. Yang and L. Hu, Scalable and highly efficient mesoporous wood-based solar steam generation device: Localized heat, rapid water transport, *Advanced Functional Materials*, **28**, 2018, pp. 1707134 (doi:10.1002/adfm.201707134).
[13] X. Wang, Q. Liu, S. Wu, B. Xu and H. Xu, Multilayer polypyrrole nanosheets with self-organized surface structures for flexible and efficient solar-thermal energy conversion, *Advanced Materials*, **31**, 2019, pp. e1807716 (doi:10.1002/adma.201807716).
[14] P. Tao, G. Ni, C. Song, W. Shang, J. Wu, J. Zhu, G. Chen and T. Deng, Solar-driven interfacial evaporation, *Nature Energy*, **3**, 2018, pp. 1031-1041 (doi:10.1038/s41560-018-0260-7).
[15] L. Zhang, Z. Xu, L. Zhao, B. Bhatia, Y. Zhong, S. Gong and E. N. Wang, Passive, high-efficiency thermally-localized solar desalination, *Energy & Environmental Science*, **14**, 2021, pp. 1771-1793 (doi:10.1039/d0ee03991h).
[16] H. Shen, Z. Zheng, H. Liu and X. Wang, A solar-powered interfacial evaporation system based on MoS_2-decorated magnetic phase-change microcapsules for sustainable seawater desalination, *Journal of Materials Chemistry A*, **10**, 2022, pp. 25509-25526 (doi:10.1039/d2ta07353f).
[17] J. He, N. Li, S. Wang, S. Li, J. Li, L. Yu, S. Liu, P. Murto and X. Xu, Efficient solar-powered interfacial evaporation, water remediation, and waste conversion based on a tumbler-inspired, all-cellulose, and monolithic design, *Advanced Sustainable Systems*, **6**, 2022, pp. 2200256 (doi:10.1002/adsu.202200256).
[18] X. Zhao, X. Meng, H. Zou, Z. Wang, Y. Du, Y. Shao, J. Qi and J. Qiu, Topographic manipulation of graphene oxide by polyaniline nanocone arrays enables high-performance solar-driven water evaporation, *Advanced Functional Materials*, **33**, 2022, pp. 2209207 (doi:10.1002/adfm.202209207).

[19] S. Loeb, C. Li and J. H. Kim, Solar photothermal disinfection using broadband-light absorbing gold nanoparticles and carbon black, *Environmental Science & Technology*, **52**, 2018, pp. 205-213 (doi:10.1021/acs.est.7b04442).

[20] H. Chen, S.-L. Wu, H.-L. Wang, Q.-Y. Wu and H.-C. Yang, Photothermal devices for sustainable uses beyond desalination, *Advanced Energy and Sustainability Research*, **2**, 2021, pp. 2000056 (doi:10.1002/aesr.202000056).

[21] Z. C. Xiong, Y. J. Zhu, D. D. Qin and R. L. Yang, Flexible salt-rejecting photothermal paper based on reduced graphene oxide and hydroxyapatite nanowires for high-efficiency solar energy-driven vapor generation and stable desalination, *ACS Applied Materials & Interfaces*, **12**, 2020, pp. 32556-32565 (doi:10.1021/acsami.0c05986).

[22] L. Yang, G. Chen, N. Zhang, Y. Xu and X. Xu, Sustainable biochar-based solar absorbers for high-performance solar-driven steam generation and water purification, *ACS Sustainable Chemistry & Engineering*, **7**, 2019, pp. 19311-19320 (doi:10.1021/acssuschemeng.9b06169).

[23] Y. Li, C. Xiong, H. Huang, X. Peng, D. Mei, M. Li, G. Liu, M. Wu, T. Zhao and B. Huang, 2D $Ti_3C_2T_x$ MXenes: Visible black but infrared white materials, *Advanced Materials*, **33**, 2021, pp. e2103054 (doi:10.1002/adma.202103054).

[24] J. Luo, L. Yang, D. Sun, Z. Gao, K. Jiao and J. Zhang, Graphene oxide "surfactant"-directed tunable concentration of graphene dispersion, *Small*, **16**, 2020, pp. e2003426 (doi:10.1002/smll.202003426).

[25] B. Han, Y.-L. Zhang, Q.-D. Chen and H.-B. Sun, Carbon-based photothermal actuators, *Advanced Functional Materials*, **28**, 2018, pp. 1802235 (doi:10.1002/adfm.201802235).

[26] C. Chen, M. Wang, X. Chen, X. Chen, Q. Fu and H. Deng, Recent progress in solar photothermal steam technology for water purification and energy utilization, *Chemical Engineering Journal*, **448**, 2022, pp. 137603 (doi:10.1016/j.cej.2022.137603).

[27] X. Liu, F. Chen, Y. Li, H. Jiang, D. D. Mishra, F. Yu, Z. Chen, C. Hu, Y. Chen, L. Qu and W. Zheng, 3D hydrogel evaporator with vertical radiant vessels breaking the trade-off between thermal localization and salt resistance for solar desalination of high-salinity, *Advanced Materials*, **34**, 2022, pp. e2203137 (doi:10.1002/adma.202203137).

[28] Z. Yu and P. Wu, Biomimetic MXene-polyvinyl alcohol composite hydrogel with vertically aligned channels for highly efficient solar steam generation, *Advanced Materials Technologies*, **5**, 2020, pp. 2000065 (doi:10.1002/admt.202000065).

[29] Y. Zou, J. Zhao, J. Zhu, X. Guo, P. Chen, G. Duan, X. Liu and Y. Li, A mussel-inspired polydopamine-filled cellulose aerogel for solar-enabled water remediation, *ACS Applied Materials & Interfaces*, **13**, 2021, pp. 7617-7624 (doi:10.1021/acsami.0c22584).

[30] Z. C. Xiong, Y. J. Zhu, Z. Y. Wang, Y. Q. Chen and H. P. Yu, Tree-inspired ultralong hydroxyapatite nanowires-based multifunctional aerogel with vertically aligned channels for continuous flow catalysis, water disinfection, and solar energy-driven water purification, *Advanced Functional Materials*, **32**, 2021, pp. 2106978 (doi:10.1002/adfm.202106978).

[31] W. Xu, Y. Xing, J. Liu, H. Wu, Y. Cui, D. Li, D. Guo, C. Li, A. Liu and H. Bai, Efficient water transport and solar steam generation *via* radially, hierarchically structured aerogels, *ACS Nano*, **13**, 2019, pp. 7930-7938 (doi:10.1021/acsnano.9b02331).

[32] X. Lin, P. Wang, R. Hong, X. Zhu, Y. Liu, X. Pan, X. Qiu and Y. Qin, Fully lignocellulosic biomass-based double-layered porous hydrogel for efficient solar steam generation, *Advanced Functional Materials*, **32**, 2022, pp. 2209262 (doi:10.1002/adfm.202209262).

[33] S. Chaule, J. Hwang, S. J. Ha, J. Kang, J. C. Yoon and J. H. Jang, Rational design of a high performance and robust solar evaporator *via* 3D-printing technology, *Advanced Materials*, **33**, 2021, pp. e2102649 (doi:10.1002/adma.202102649).

[34] Z. Sun, J. Wang, Q. Wu, Z. Wang, Z. Wang, J. Sun and C. J. Liu, Plasmon based double-layer hydrogel device for a highly efficient solar vapor generation, *Advanced Functional Materials*, **29**, 2019, pp. 1901312 (doi:10.1002/adfm.201901312).

[35] P. Zhang, F. Liu, Q. Liao, H. Yao, H. Geng, H. Cheng, C. Li and L. Qu, A microstructured graphene/poly(N-isopropylacrylamide) membrane for intelligent solar water evaporation, *Angewandte Chemie-International Edition*, **57**, 2018, pp. 16343-16347 (doi:10.1002/anie.201810345).

[36] H. W. Lim and S. J. Lee, Double-insulated porous PDMS sponge for heat-localized solar evaporative seawater desalination, *Desalination*, **526**, 2022, pp. 115540 (doi:10.1016/j.desal.2021.115540).
[37] P. Song, Z. Xu, Y. Wu, Q. Cheng, Q. Guo and H. Wang, Super-tough artificial nacre based on graphene oxide *via* synergistic interface interactions of π-π stacking and hydrogen bonding, *Carbon*, **111**, 2017, pp. 807-812 (doi:10.1016/j.carbon.2016.10.067).
[38] Y. Kuang, C. Chen, G. Chen, Y. Pei, G. Pastel, C. Jia, J. Song, R. Mi, B. Yang, S. Das and L. Hu, Bioinspired solar-heated carbon absorbent for efficient cleanup of highly viscous crude oil, *Advanced Functional Materials*, **29**, 2019, pp. 1900162 (doi:10.1002/adfm.201900162).
[39] Z. Lei, S. Zhu, X. Sun, S. Yu, X. Liu, K. Liang, X. Zhang, L. Qu, L. Wang and X. Zhang, A multiscale porous 3D-fabric evaporator with vertically aligned yarns enables ultra-efficient and continuous water desalination, *Advanced Functional Materials*, **32**, 2022, pp. 2205790 (doi:10.1002/adfm.202205790).
[40] Y. Guo, X. Zhou, F. Zhao, J. Bae, B. Rosenberger and G. Yu, Synergistic energy nanoconfinement and water activation in hydrogels for efficient solar water desalination, *ACS Nano*, **13**, 2019, pp. 7913-7919 (doi:10.1021/acsnano.9b02301).